Numerical simulation and experimental study on non-uniform strain during hot compression of aluminium alloy

Haigen Jian, Yedong Wang, Xiaomei Yang, Chengji Mi* and Xinlei Lei

School of Materials and Advanced Manufacturing,
Hunan University of Technology,
Zhuzhou, 412007, China
Email: jianhaigen2001@163.com
Email: 1204197225@qq.com
Email: 1334731734@qq.com
Email: 1992623753@qq.com
Email: 3351388941@qq.com
*Corresponding author

Wei Zhang

Hunan Esoe Intelligent Manufacturing Co., Ltd.,
Zhuzhou, 412007, China
Email: 68357964@qq.com

Abstract: The finite element numerical simulation of hot compression deformation process of B93 aluminium alloy was carried out by *DEFORM-3D* software. Besides, the microstructure characteristics of deformed specimens in different regions and the relationship between non-uniform strain and dynamic recrystallisation during deformation were analysed by experimental study. The results show that the hot compression process of B93 aluminium alloy obviously exhibits a nonuniform characteristic of deformation, the region with the largest equivalent strain is the most prone to deformation. Also, in the largest equivalent strain zone, dynamic recrystallisation reacts the most complete, and the grain size reaches the minimum value. Nonuniform deformation show a rising tendency with the increase of strain rate and deformation temperature, and the influence of strain rate on nonuniform deformation is slightly greater than that of deformation temperature. The most suitable hot working process for the alloy is 410~430°C/0.001~0.01s^{-1}.

Keywords: B93 aluminium; numerical simulation; hot deformation; equivalent strain; finite element analysis; effective plastic strain; dynamic recrystallisation; grain size; strain rate; nonuniform deformation.

Reference to this paper should be made as follows: Jian, H., Wang, Y., Yang, X., Mi, C., Lei, X. and Zhang, W. (2021) ‘Numerical simulation and experimental study on non-uniform strain during hot compression of aluminium alloy’, *Int. J. Computational Materials Science and Surface Engineering*, Vol. 10, No. 1, pp.13–26.

Biographical notes: Haigen Jian is an Associate Professor of Hunan University of Technology, mainly engaged in the research of aluminium alloy microstructure.

Yedong Wang, Master of Hunan University of Technology, mainly engaged in the research of electrochemical corrosion and protection of aluminium alloys.

Xiaomei Yang, Master of Hunan University of technology, mainly engaged in the research of electrochemical corrosion and protection of aluminium alloys.

Chengji Mi is Professor of Hunan University of technology, mainly engaged in the research of electrochemical corrosion and protection of aluminium alloys.

Xinlei Lei is a student of Hunan University of Technology.

Wei Zhang is Senior Engineer of Hunan Esoe Intelligent Manufacturing Co., Ltd.

1 Introduction

In modern physical simulating technique field, thermal and mechanical simulation testing machine is used to test small samples, which can quickly and accurately study the change rule of material performance and microstructure under the approximate actual situation. Therefore, the physical simulating technique has attracted extensive attention in the field of material engineering. Pressure processing is one of the most important fields in the research of thermal processing technology as a physical simulation technology. The purpose of the pressure processing is to determine the optimum processing parameters of materials according to the characteristics that different structures and properties of materials can be obtained by thermal compression deformation under different conditions (Shen and Xie, 2000; Lin and Chen, 2011; Niu, 2007). However, in the process of thermal compression of cylindrical specimens, due to the large friction at the end surface, the specimen would experience uneven deformation, which makes the cylindrical specimens are big in the middle but is small at both ends, and show the shape of waist drum. The inhomogeneity of deformation would directly affect the precipitation kinetics, deformation recrystallisation of materials, which will lead to the inhomogeneity of the properties and microstructures of corresponding regions (Wei et al., 2006; Du et al., 2007). Therefore, making a deep study of the non-uniformity and regularity of deformation in the longitudinal section of the specimen during hot compression has an important significance in guiding the practice of physical simulation.

With the rapid development of computer technology, finite element software such as *DEFORM*, *ABAQUS*, *COMSOL* Multiphysics are more and more widely used in the field of scientific research and engineering. Finite element simulation can effectively improve work efficiency by transforming mathematical equations into digital images to describe physical phenomena in the process of material deformation. The combination of experimental data and finite element simulation is an effective way to study the non-uniform deformation of materials during thermal compression (Lan et al., 2001; Gronostajski, 2000).

In this paper, the hot compression test of B93 aluminium alloy was carried out by *Gleeble-3800* thermal simulation tester; the experimental conditions are as follows: deformation temperature is 350~470°C, deformation rate is 0.001~10 s^{-1}, and deformation amount is within 50%. Based on the experimental data, *DEFORM-3D* finite element model was established, and the thermal compression deformation of B93 aluminium alloy was simulated by software. Also, the inhomogeneity of strain field under different temperatures and strain rates was analysed by post-processing program, which provided a reference for the study of inhomogeneity of the material physical simulation process. At the same time, the characteristics of microstructure change and the relationship between deformation conditions and microstructure of B93 aluminium alloy during high-temperature deformation were studied, and the processing maps of B93 aluminium alloy were calculated and analysed according to the dynamic materials model (*DMM*) (Prasad et al., 1984). The flow instability areas of B93 aluminium alloy during hot deformation were determined by processing maps, and the optimum technological parameters of B93 aluminium alloy during hot deformation were finally obtained.

2 Experimental materials and methods

2.1 Materials and methods

In this paper, taking B93 high strength aluminium alloy ingot fabricated by semi-continuous casting as the test materials, and the chemical composition of B93 aluminium alloy are as follows: *w* (Zn) = 6.5%, *w* (Mg) = 1.8%, *w* (Cu) = 1.2%, *w* (Fe) = 0.3%, *w* (Si) = 0.1%, and the rest is Al. The microstructure observation results of the ingot are shown in Figure 1, which shows the average grain size is about 100μm, and some dendrite structures can be observed (Figure 1(a)). When the scanning electron microscope was magnified by 2000 times, skeletal and massive phases can be clearly observed along the grain boundary. Energy spectrum analysis shows that the skeletal phase is mainly η phase ($MgZn_2$) and T phase (AlZnMgCu), while the massive phase is Al_6 (CuFe). The aluminium alloy ingot was processed into a cylindrical sample of 10mm×12mm along the axial direction of the ingot, and then the alloy sample was subjected to homogenisation treatment at the temperature of 360°C/24h. The isothermal compression test of B93 aluminium alloy was carried out on Gleeble-3800 thermal simulation tester; the experimental conditions are as follows: heating rate is 2°C/s, holding time is 3 min, and deformation amount is 50%. In addition, the compression temperatures are 350°C, 380°C, 420°C, 450°C, and 470°C respectively, and the strain rates are 0.001 s^{-1}, 0.01 s^{-1}, 0.1 s^{-1}, 1 s^{-1} and 10 s^{-1} respectively. In the process of compression, graphite sheets were added at both ends of the specimen and lubricant was evenly coated on the specimen to reduce friction. According to the data of physical simulation experiment, the stress-strain curves and constitutive equation of the B93 aluminium alloy are shown in Figure 2 and formulae (1) respectively (Jan et al., 2011):

$$\varepsilon = 1.58 \times 10^{15}[\sinh(0.00981\sigma)^{7.91}\exp(-265.49/RT) \tag{1}$$

Note: ε is the deformation rate, σ is the rheological stress, R is the molar gas constant, and T is the deformation temperature.

Figure 1 The microstructure of as-cast B93 alloy (see online version for colours)

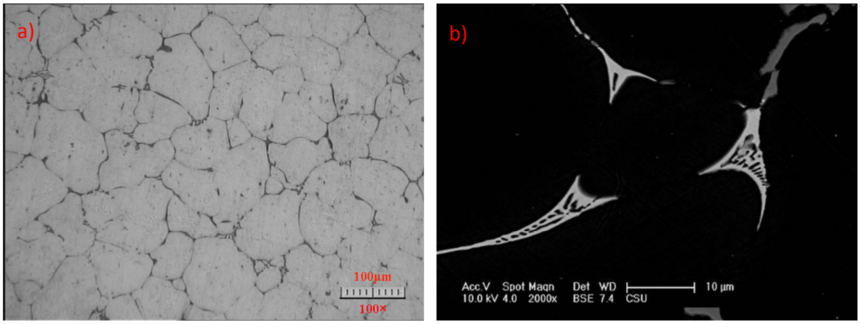

Figure 2 The stress-strain curves of aluminium alloy under different hot compression conditions: (a) 0.001 s^{-1}; (b) 0.01 s^{-1}; (c) 0.1 s^{-1}; (d) 1 s^{-1} and (e) 10 s^{-1} (see online version for colours)

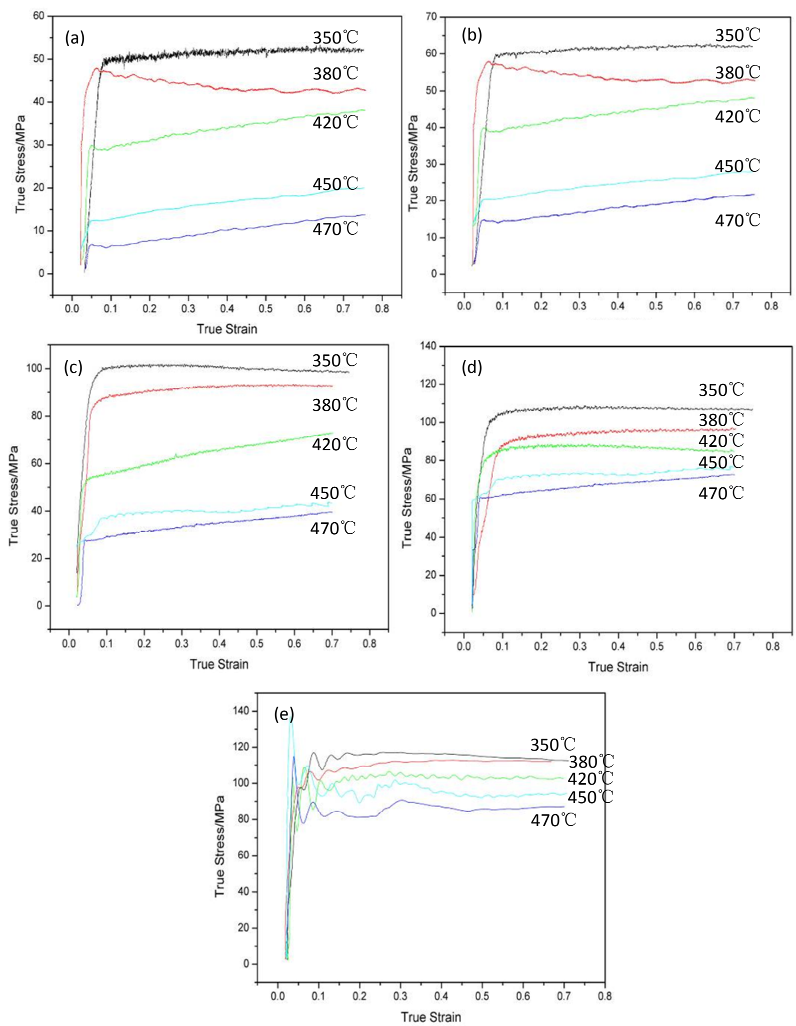

2.2 Finite element simulation

In the whole hot compression process, owing to the materials of the upper and lower die were steel and the deformation could be neglected, so it was set as a rigid body. The test material is B93 ingot with the elastic modulus, density and friction coefficient with die steel of 71.7 GPa, 2.81 g/cm^3 and 0 respectively, which was set as rigid-plastic body. In this paper, the tetrahedral mesh divider in *DEFORM-3D* software was used to control the number and size of the grid at the same time. The ratio of the maximum size to the minimum size of the element was set to 1, and the sample was divided into 20,000 grids. Due to the symmetry of the specimen, only 1/4 of the specimen was selected for simulation observation, as shown in Figure 3. In the whole simulation process, the total number of steps is set to 100 and saved every ten steps. The numerical simulation method adopts the conjugate gradient iterative method, and the iterative method adopts the direct iteration method (Li et al., 2012; Sun et al., 2005).

Figure 3 Finite element graticule of the model (see online version for colours)

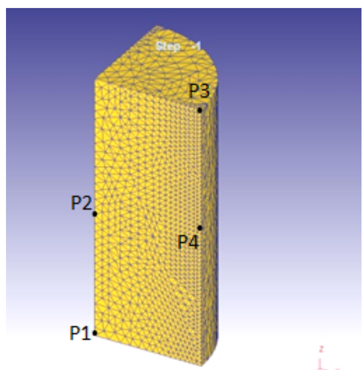

3 Numerical simulation and experimental results

3.1 Analysis of finite element simulation results

The thermal compression tests with deformation temperature of 350°C~450°C and deformation rate of 0.001~1 s^{-1} were researched by finite element simulation. The distribution map of an equivalent strain of specimens at different temperatures and strain rates are shown in Figure 4, and the compression direction is the *Z* direction. From Figure 4, it could be seen clearly that the equivalent strain of the specimen has the same distribution law under different deformation conditions. However, after thermal compression, the strain distribution of each sample turns to be inhomogeneous, which is mainly due to the existence of large friction forces between the end face of the sample and the indenter. Moreover, compared with other areas of the specimen, the metal fluidity in the centre of the end face of the specimen is more lower. After deformation, the upper and lower end faces of the specimen become smaller, while the middle of the specimen protrudes outward, eventually, the shape of the specimen looks like a waist drum.

The equivalent strain values of the key points of the specimen under different hot compression deformation conditions (P1–P4 point in Figure 3) are compared and analysed, and the results are shown in Table 1. Nonuniform deformation shows a rising tendency with the increase of strain rate and deformation temperature. For example, at the central position of the sample (P2 point), when the strain rate is 0.001 s^{-1}, the strain increases from 0.681 at 350°C to 0.713 at 420°C. When the deformation temperature is 420°C, with the growth of strain rate from 0.001 s^{-1} to 1 s^{-1}, the strain also increases from 0.713 to 0.765.

Table 1 The strain values of the key points of the specimen under different conditions

Deformation conditions	*P1*	*P2*	*P3*	*P4*
350°C/0.001 s^{-1}	0.072	0.681	1.363	0.164
420°C/0.001 s^{-1}	0.081	0.713	1.382	0.171
420°C/1 s^{-1}	0.092	0.765	1.451	0.193
450°C/1 s^{-1}	0.100	0.791	1.533	0.221

Figure 4 Distribution map of strain-effective for specimens under various hot compression conditions: (a) 350°C/0.001 s^{-1}; (b) 420°C/0.001 s^{-1}; (c) 420°C/1 s^{-1} and (d) 450°C/1 s^{-1} (see online version for colours)

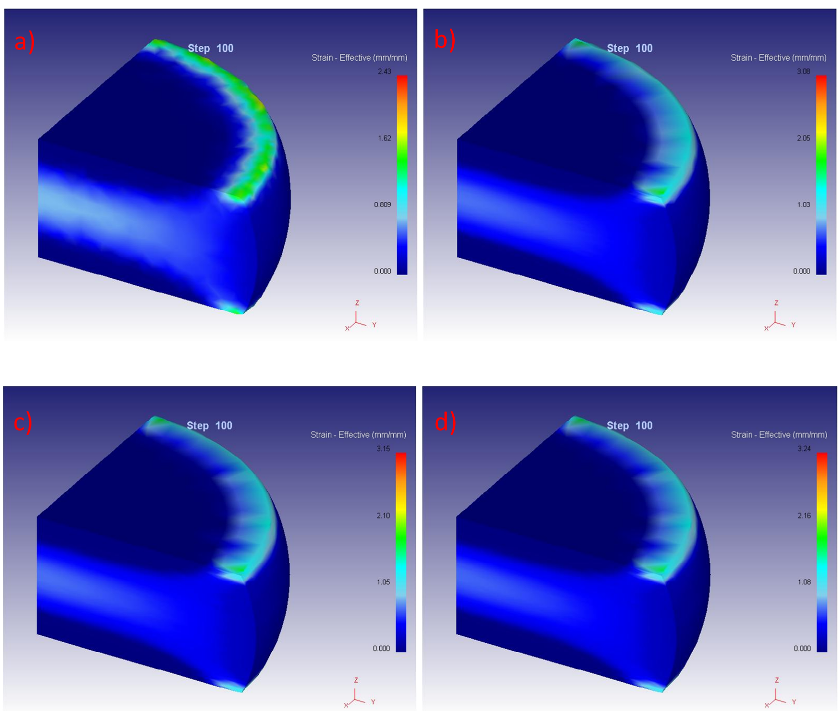

According to the degree of deformation in different deformation zones after compression, the specimens are divided into four zones, as shown in Figure 5. Taking the hot compression sample with deformation condition of 420°C/0.001 s^{-1} as an example, the equivalent strain of four key points in Figure 3 are analysed. The results show that the strain in different deformation regions is different. The strain value in the edge area of the end face of the hot compression specimen is the largest, which belongs to the easy deformation region, such as the point P3, the strain value is 1.382. The strain value in the centre region of the specimen is slightly lower than that in the edge region of the end surface of the specimen, which belongs to the free deformation zone, such as the point P2, the strain value is 0.713. The strain value of cylindrical waist drum position has a low value, such as the point P4, the strain value is 0.171. However, the strain value in the central area of the end face of the specimen is the smallest, which belongs to the difficult deformation zone, such as the point P1, only 0.081.

Continue to study the changes of strain values at the four points mentioned above, and making an in-depth analysis of the changes of strain values with time. The results are shown in Figure 6. In the early stage of thermal compression, the strain value of different regions increase slowly, and the strain of different regions have little difference. With the increase of deformation, the strain value at point P3 increases the fastest, and the value is the largest. The strain values at point P1 almost keep the same level, which indicates that no obvious deformation occurs at this point. There is no obvious deformation at P4, and its strain value is only slightly larger than that at P1, while the strain at P2 point in the centre of the sample increases linearly. It could thus be concluded that the deformation of the various regions during the thermal compression of the sample exhibits a nonuniform characteristic of deformation.

Figure 5 Schematic diagram of the deformation area of hot compression specimen

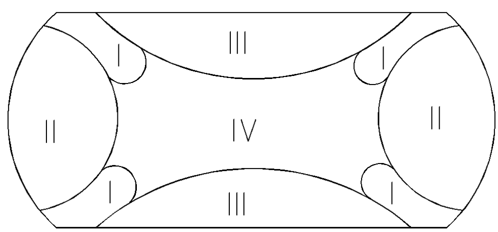

Figure 6 Variation curve of the strain with time (420°C, 0.001 s^{-1}) (see online version for colours)

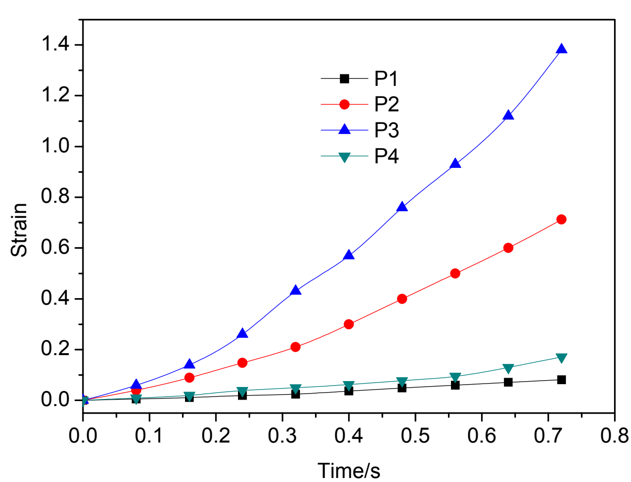

In general, the initial nucleation of dynamic recrystallisation is closely related to strain. Dynamic recovery and dynamic recrystallisation often occur in the thermal deformation process of materials. On the one hand, dislocations accumulate continuously with the increase of deformation amount, which results in work hardening of materials. On the other hand, dislocations disappear and form subcrystal through thermal activation, which softens the materials. In the early stage of hot compression, the dynamic recrystallisation would not occur because of the small dislocation density. But with the increase of deformation, dynamic recrystallisation would occur when the dislocation accumulates to a certain extent (Inoue, 2000). From the simulation results, it could be seen that the strain value at P1 is always very small during compression deformation and is in a state of working hardening. With the prolongation of time, the strain values of P3 and P2 increases rapidly, and dynamic crystallisation could occur in a short time.

3.2 Analysis of experimental results

To intuitively understand the deformation of each region of the specimen after hot compression deformation, the hot compression sample with a deformation condition of 420°C/0.001 s^{-1} was cut and polished along the loading direction, and the metallographic structure was observed after corrosion. The microstructure and morphology of different regions are obtained, as shown in Figure 7.

Figure 7 Metallographic structure of different regions of the hot compression specimens (420°C/0.001 s^{-1}): (a) Zone 1; (b) Zone 2; (c) Zone 3 and (d) Zone 4 (see online version for colours)

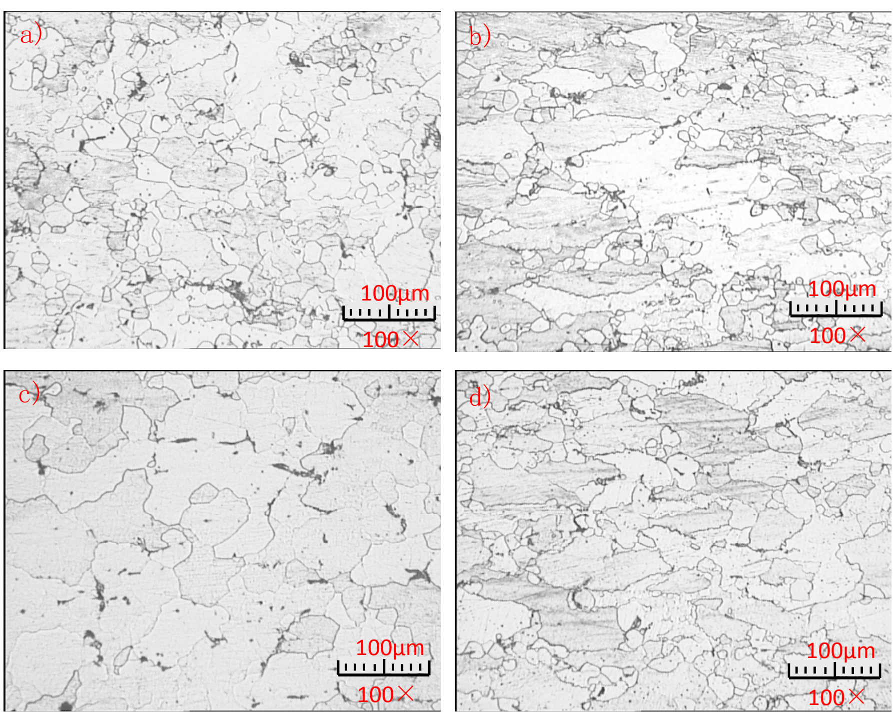

As can be seen from Figure 7, the grain size of the region I is very small and uniform, and a small amount of equal-axis grains are scattered in the region I, which indicates that region I has a relatively complete dynamic recrystallisation structure and the growing degree of recrystallisation grains to be low. The grain size of region II is larger and uneven than that of region I, and the shape of large grain in the region II is flat, which shows that the degree of dynamic recrystallisation in this region is low. Compared with other regions, the grain size of zone III is the largest and grains present an equiaxed shape. This is because the strain in zone III during deformation is very small and does not reach the critical strain ε_c required for dynamic recrystallisation, so there is no dynamic recrystallisation. Similarly, because the strain is very small, the possibility of flattening the original grain is also very slight, so the grains still present an equiaxed shape (Zhenbo et al., 2011). The grain size of zone IV is larger than that of zone I, but smaller than that of zone II and III, and the crystal grains distribution is not so uniform. There are some flattened crystal grains with a slightly larger size in the zone IV; at the same time, some smaller equiaxed grains are distributed around the flattened large grains. All of these illustrate that incomplete dynamic recrystallisation occurs during deformation in the zone III, and the degree of recrystallisation is greater than that in regions II and III.

To have a better understand of the effect of non-uniform strain on dynamic recrystallisation, the relationship between recrystallisation degree and equivalent strain in different regions was studied. The results are shown in Table 2. It could be found that there is a positive correlation between the degree of dynamic recrystallisation and the size of equivalent strain, in other words, the degree of dynamic recrystallisation increases with the equivalent strain increase, and decreases with the equivalent strain decrease.

Table 2 The relationship between recrystallisation degree and equivalent strain in different regions under different deformation conditions

Zone	*I*	*II*	*III*	*IV*
The degree of dynamic recrystallisation	Fully recrystallisation	Relatively low	Non-recrystallisation	Relatively high
The value of equivalent strain	Maximum	Relatively small	Minimum	Relatively large

Under different deformation conditions, the scanning morphology of the waist drum position (P4 point) of the specimen after hot compression deformation is shown in Figure 8. The surface strain of the sample increases with the temperature and strain rate increase; in other words, the tendency of hot cracks of hot compressed specimens increased by deformation fluctuation degree. During hot compression, work hardening and dynamic softening compete with each other. With the increase of strain rate, dislocation density, dislocation accumulation and tangle also increase, meanwhile, with the increase of strain rate, vacancy concentration and deformation resistance also increase, which makes the specimen more prone to cracking. With the increase of deformation temperature, skeletal η ($MgZn_2$) phase and T (AlZnMgCu) phase will dissolve on the grain boundary, but the re-dissolution effect of these phases is limited due to the short compression deformation time. However, the bulk Al_6 (CuFe) phase is difficult to occur re-dissolution phenomenon due to having good thermal stability. In the process of hot compression deformation, these coarse intergranular phases are easy to induce microcracks under high stress, which results in grain boundary cracking. So, the hot compression sample with a deformation condition of 420°C/0.001 s^{-1} appears more obvious grain boundary cracking phenomenon, As shown in Figure 8(d).

Figure 8 SEM images of specimens under various hot compression conditions: (a) 350°C/0.001 s^{-1}; (b) 420°C/0.001 s^{-1}; (c) 420°C/1 s^{-1} and (d) 450°C/1 s^{-1} (see online version for colours)

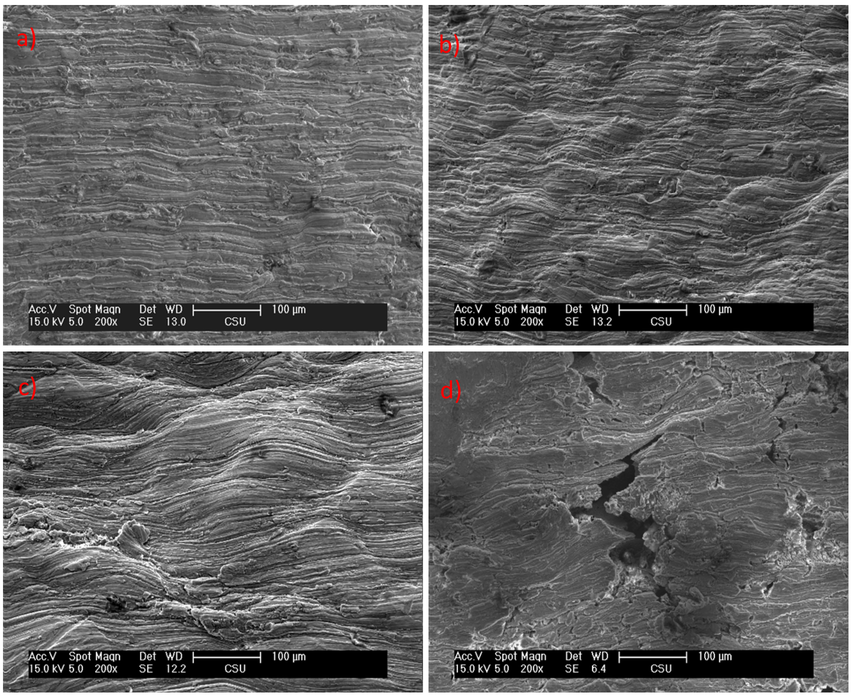

In order to optimise hot processing parameters of B93 aluminium alloy and define the unstable rheological region of B93 aluminium alloy after hot compression, we will make further analysis about it according to relevant theories. According to the dynamic material model proposed by Parasad (Prasad et al., 1984), the workpiece used for thermal deformation was regarded as an energy dissipation model, during the process of plastic deformation, the total energy P of the external input workpiece is mainly consumed in the following two aspects: the first part is the energy g consumed by the plastic deformation of the workpiece; the second part is the energy J consumed by microstructure evolution during the deformation process.

$$P = \sigma \cdot \dot{\varepsilon} = G + J = \int_0^{\dot{\varepsilon}} \sigma \mathrm{d}\dot{\varepsilon} + \int_0^{\sigma} \dot{\varepsilon} \mathrm{d}\sigma \tag{2}$$

The ratio of these two energies is determined by the strain rate sensitivity index m of the material under certain stress conditions:

$$m = \frac{dJ}{dG} = \frac{\dot{\varepsilon} d\sigma}{\sigma d\dot{\varepsilon}} = \frac{d \log \sigma}{d \log \dot{\varepsilon}} \tag{3}$$

When the instability diagram is superimposed on the power dissipation diagram, we will get the processing diagram. The power dissipation diagram represents the power dissipation when the material fibre structure changes, and it's change rate can be expressed by a dimensionless parameter η, Where m is the strain rate sensitivity index.

$$\eta = \frac{2m}{m+1} \tag{4}$$

Based on the principle of irreversible thermodynamic extremum, the instability diagram attempts to use another dimensionless parameter $\xi(\dot{\varepsilon})$ to express the criterion of continuous instability in large plastic flow:

$$\xi(\dot{\varepsilon}) = \frac{\partial \ln[m/(m+1)]}{\partial \ln \dot{\varepsilon}} + m \tag{5}$$

When $\xi(\dot{\varepsilon}) < 0$, it is in an unsteady rheological state. The variable $\xi(\dot{\varepsilon})$ containing temperature and strain rate finally forms the instability diagram, and the instability region can be determined by superimposing the instability diagram on the power dissipation diagram.

By overlapping the power dissipation diagram calculated by formula (4) with the instability diagram calculated by formula (5), eventually, the processing maps of B93 aluminium alloy with strains of 0.1, 0.3 and 0.5 can be got by the Matlab, As shown in Figure 9, in which the power dissipation coefficient is represented by the number on the contour line.

According to the results of the stress-strain curve (Jan et al., 2011), in the range of deformation temperature 300–470°C and strain rate 0.001–10 s^{-1}, the processing map of strain 0.1 represents the state of transition deformation, the processing map of the strain 0.3 represents the state of peak stress, and the processing map of strain 0.5 represents the state of steady-state rheological. Comparing Figure 9(a), (b) with (c), it could be seen that there is no instability region in the processing map with the strain of 0.1. But, when the strain rate is higher than 1 s^{-1}, the processing map with strain of 0.3 appears obvious deformation instability phenomenon in the whole temperature range. When the temperature is lower than 400°C, and the strain rate is higher than 0.1 s^{-1}, the processing map with the strain of 0.5 appears more obvious deformation instability phenomenon under high temperature and high strain rate conditions.

In the actual production process, the strain of the alloy in the subsequent extrusion, forging and other processing processes is larger, so the security zone in the processing map with the strain of 0.5 (Figure 9(c)) is selected for in-depth analysis. There are three regions with large power dissipation coefficient in the processing map with the strain of 0.5. The maximum power dissipation coefficient of each region is about 0.3, and the temperature of each region is about 300°C ('low temperature'), 420°C ('medium temperature') and 470°C ('high temperature') respectively. In the lower temperature region, such as the region with the deformation temperature about 300°C and the strain rate about 0.01 s^{-1} is the warm-working area of B93 aluminium alloy. Moreover, artificial ageing has an important influence on the final capabilities of B93 aluminium Products. However, this method is generally not used in the actual production process. At high temperature, the maximum power dissipation coefficient of B93 aluminium alloy is about 0.34, and the aluminium alloy is easy to fracture in the process of deformation. Therefore, it is not suitable for hot working of the alloy in a high-temperature zone. The middle temperature region with the deformation temperature about 420°C and the strain rate about 0.001 s^{-1} is the heat deformation region of B93 aluminium alloy. At this time, the maximum power dissipation coefficient of the alloy is about 0.34. Therefore, the subsequent extrusion, forging and other processes of the alloy could be carried out in the middle temperature region, which is well proved by the observation results of the morphology of the waist drum position of the sample after hot working (Figure 8).

Figure 9 Processing diagrams of B93 aluminium alloy under different strain conditions: (a) $\varepsilon = 0.1$; (b) $\varepsilon = 0.3$ and (c) $\varepsilon = 0.5$ (see online version for colours)

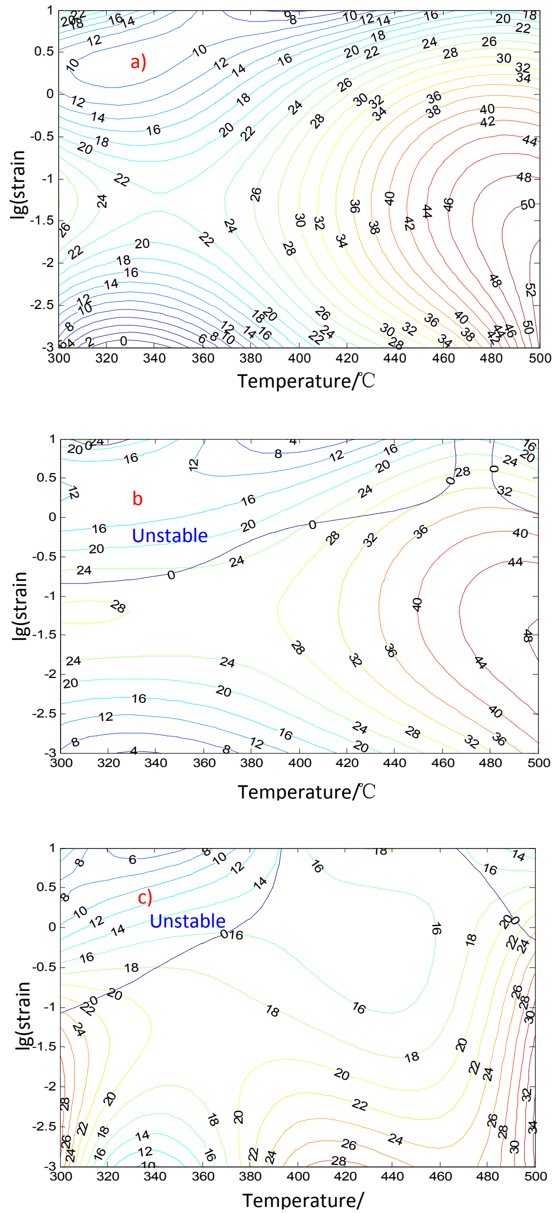

4 Conclusion

The microstructure change characteristics of B93 aluminium alloy under different deformation temperature (350~470°C) and deformation rate (0.001–1 s~10 s^{-1}) are analysed by means of finite element numerical simulation and experimental observation. The results show that:

1. The hot compression process of B93 aluminium alloy obviously exhibits a nonuniform characteristic of deformation. The edge area of the end face of the cylindrical specimen belongs to the easy deformation region, however, the region near the location of the cylindrical waist drum is difficult to deformation in the process of hot compression. The results show that the higher the temperature and the higher the strain rate, the more obvious the waist drum shape of the sample is. The hot compression sample with a deformation condition of 420°C/0.001 s–1 appears more obvious grain boundary cracking phenomenon.
2. The non-uniform strain of the sample has a significant influence on the dynamic recrystallisation of the alloy, and the degree of dynamic recrystallisation is positively related to the equivalent strain.
3. The deformation resistance of B93 aluminium alloy is high during low-temperature compression, and hot cracks are easy to occur on the surface of the alloy due to crystal boundary weakening during high-temperature compression. The hot deformation and processing of B93 aluminium alloy is particularly well adapted in the medium temperature region, the optimum hot working temperature range is 410 ~430°C, and the strain rate range is 0.001 ~0.01 s^{-1}.

Acknowledgements

This work was financially supported by the Natural Science Foundation of Hunan Province (2018JJ4060), China Students project for innovation and entrepreneurship training (201811535021)and Hunan Province college students research learning and innovative experiment project (2018660).

References

Du, F.S., Wang, M.T. and Li, X.T. (2007) 'Research on deformation and microstructure evolution during forging of large-scale parts source', *J. Mater Process Technol.*, Vol. 187, pp.591–594.

Gronostajski, Z. (2000) 'The constitutive equations for FEM analysis', *J. Mater Process Technol*, Vol. 106, pp.40–44.

Inoue, T. (2000) 'Effect of shear deformation on refinement of crystal grains', *Mater Sci Technol*, Vol. 18, pp.1007–1015.

Jan, H.G., Jiang, F. and Zheng, X.Y. (2011) 'Hot deformation behavior of high strength and toughness B93 aluminum alloy', *J. Cent South Univ*, Vol. 42, pp.2291–2296.

Lan, Y.J., Chen, X.Y. and Huang, C.J. (2001) 'Numerical simulation and experimental verification of temperature distribution in hot-rolling strip steel', *Acta Metall Sin*, Vol. 37, pp.99–103.

Li, J.L., Jiang, F. and Jian, H.G. (2012) 'Study on simulation of hot processing behavior of B93 aluminum alloy', *J. Aeronaut Mater*, Vol. 32, pp.20–25.

Lin, Y.C. and Chen, X.M. (2011) 'A critical review of experimental results and constitutive descriptions for metals and alloys in hot working', *Mater Des*, Vol. 32, pp.1733–1759.

Niu, J.T. (2007) *Physical Simulation in Materials and Hot-Working* (National Defense Industry Press, China).

Prasad, Y.V.R.K., Gegel, H.L. and Doraivelu, S.M. (1984) 'Medeling of dynamic material behavior in hot deformation: forging of Ti-6242', *Metall Trans. A.*, Vol. 15, pp.1883–1892.

Shen, J. and Xie, S.S. (2000) 'Dynamic recovery and dynamic recrystallization of 7005 aluminum alloy during hot compression', *Acta Metall Sin*, Vol. 13, pp.379–386.

Sun, S.H., Xiong, Y. and Zhao, J. (2005) 'Microstructure characteristics in high carbon steel rod after warm cross-wedge rolling', *Scripta Mater*, Vol. 53, pp.137–140.

Wei, J., Li, Q. and Tang, G.B. (2006) 'Physical simulation in materials and hot-working investigation on relationship of uneven strain and recrystallization during C-Mn steel compression', *Iron and Steel*, Vol. 41, pp.74–78.

Zhenbo, H., Huizhong, L. and Xiaopeng, L. (2011) 'Hot deformation behavior and processing map of al-zn-mg-sc-zr alloy', *Chin J. Nonferrous Met*, Vol. 21, pp.1220–1228.